Physical Insight into the Conditions Required in the Solid-Phase Molecular Self-Assembly of SDS Revealed by Coarse-Grained Molecular Dynamics Simulation

Xiangyu Dou,[∥] Hongjun Jin,[∥] Tongyue Wu, Jianbin Huang, Bin Zhang,* Zhirong Liu, Tao Chen,* and Yun Yan*

ACCESS | Metrics & More | Article Recommendations | SI Supporting Information

ABSTRACT: Molecular self-assembled materials have attracted considerable interest in recent years. As part of the efforts to overcome the shortcoming that the solution-based methods were hardly applicable in preparing bulk macroscopic molecular self-assemblies, Yan et al. [CCS Chem. **2020**, 2, 98−106] developed a strategy of solid-phase molecular self-assembly (SPMSA) that allows scaling up the generation of massive supramolecular films. It is highly desired to understand the physical insight into the SPMSA at a molecular level. Here, in combination with the experimental study, we report molecular dynamics (MD) simulations on the SPMSA of the surfactant sodium dodecyl sulfate (SDS) using a coarse-grained method with the Martini force field model.

The MD simulations clearly manifest that a small amount of water is required to endow the SDS molecules with sufficient mobility to self-assemble, and the smaller size of the preassembled SDS particles favors their further fusion into mesophases by reducing the total surface Gibbs free energy, while the smaller interparticle distance decreases the time for the particle fusion. The simulation results agree well with the conditions required in the experiment, confirming that SMPSA is a free-energy-favored process leading to bulk self-assembled materials.
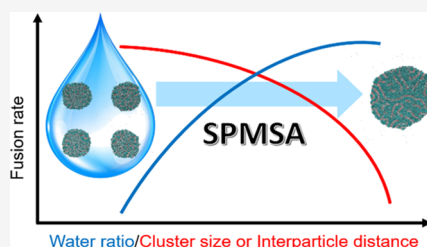
1. INTRODUCTION

Molecular self-assembly is a process in which amphiphiles spontaneously assemble to form ordered structures with unique properties.[1] Advanced intelligent materials, such as sensors,[2] photoelectric conversion devices,[3] biomedical devices,[4] luminescent materials,[5] etc., can be obtained with molecular self-assembly.[6] However, so far most molecular self-assemblies are obtained in the form of solution-based colloidal dispersions.[7−10] This solution-based molecular self-assembly is hard to work with when bulk macroscopic materials are required.[11] To tackle this problem, we recently developed a strategy of solid-phase molecular self-assembly (SPMSA),[12−17] with which supramolecular films can be obtained at large scales.[13] This not only allows the preparation of noncolloidal form self-supporting macroscopic molecular self-assembled materials but also makes it possible to achieve diversified functions.[12−14,16,17]

It was previously found that nanoscaled preassembled structure, pressure, and a small amount of water are the necessary factors for the SPMSA.[12−18] To gain more physical insights into the mechanism of the SPMSA across multiple time and space scales, in this study, we employ molecular dynamics (MD) simulations in combination with the experiment to reveal the micropictures obtained during the complicated self-assembly process. According to the time and space scale, MD simulation can be divided into quantum MD simulation (QM),[19] all-atom (AA) MD simulation,[20] and coarse-grained (CG) MD simulation. The SPMAS is related to all of the three scales, and the coarse-grained scale (μm) and all-atom scale (nm) have the closest relationship with this process.

Sodium dodecyl sulfate (SDS) is widely applied in many commercial cleaning products, such as soaps, toothpaste, etc.[17] It is also used for DNA and protein extraction[21] in polyacrylamide gel electrophoresis. Due to its common use, SDS has been extensively studied experimentally over the past century via different experimental methods.[22,23] From the perspective of colloidal chemistry, the preassemble behavior of SDS is clearly known: the formation of tail-to-tail aligned structures through hydrophobic interaction. Most importantly, we found that the SDS powders freeze-dried from their micellar solutions were able to self-assemble into a transparent macroscopic film under conditions of SPMSA, whereas both its commercial product and recrystallized products are not able to form transparent films. For this reason, it would be an ideal
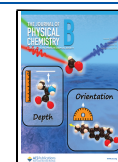
model system for us to understand the physical picture of SPMSA.

To obtain the CG force field[24] parameter, the ab initio simulation[25] was used to obtain the partial charge of the AA force field of the computational system and the all-atom optimized potentials for liquid simulations (OPLS-AA) force field[26] was used to optimize force field parameters of each bead.

2. METHODS

2.1. Experiment Details. *2.1.1. SPMSA of SDS.* To obtain the amorphous powder composed of nanometer-sized SDS domains, the 100 mM SDS aqueous solution was freeze-dried with a lyophilizer at −50 °C. Then, the powder was condensed to a white cake by finger pressing with a pressure of around 8 MPa at room temperature. Upon dropping a small amount of water onto the cake, the condensed powder was gradually transformed into a transparent film within 30 min.

2.1.2. Crystalline Samples of SDS. The commercial powder of SDS with a purity of 99.7% was dissolved in acetone and recrystallized by solvent evaporation.

2.1.3. X-ray Diffraction (XRD) Measurements. X-ray diffraction (XRD) measurements were performed on a Rigaku Dmax-2400 diffractometer with Cu Kα radiation. The solid samples were placed on clean glass slides for small-angle range tests. The lamellar period d in each sample was calculated using Bragg's Law, where $d = \lambda/2 \sin \theta$.

2.1.4. Fourier Transform Infrared Spectroscopy (FT-IR) Measurements. The FT-IR measurements of SDS were carried out on Nicolet iN10 MX microscopic infrared spectrometer (ThermoS-7 Scientific Co.) in the range of 4000−600 cm^{-1} under ambient conditions. The spectrometer was equipped with an attenuated total reflection (ATR) accessory with Smart iTR (diamond).

2.1.5. Polarized Optical Microscopy (POM) Measurement. The photographs of birefringence were captured by an LV100N polarizing microscope (Nikon Co.) in an ambient environment at room temperature. The samples were photographed with θ ranging from 0 to 359°, where θ is the angle between the analyzer and the alignment direction of the sample.

2.2. Simulation Details. To obtain the accurate CG force field parameters, ab initio simulation is used for the problems involving chemical bond fracture and electron transfer, and the full atomic partial charge of the whole system is given. Specifically, the density functional theory (DFT) calculation was employed using the 1.14*CM1A-LBCC method[27] on Lipargen.[28] The atomic charge was optimized, which is given in Table S1. With the fractional charge model obtained, the optimized OPLS-AA force field[29,30] (the final structure is given in Figure S1) simulation is thus used to study the specific molecular interaction in the SDS−H$_2$O system. Finally, the CG simulation parameters (Table S2) were optimized using the OPLS-AA force field[29] (the detailed mapping and optimized process are given in Figure S2). The motion and fusion laws of the mesoaggregates are given. Martini force field[31] with 1000 times higher calculation efficiency is employed rather than the OPLS-AA simulation.[30] The simulation results based on the optimized Martini force field of the density of SDS at 300 K agree well with experimental results obtained from literatures[32,33] (Table S3). Furthermore, the diffusion coefficients in low concentration (0.005−0.05M) was obtained based on the MD simulation, and they agree perfectly with the literature

results as well[34,35] (Figure S3). The above information qualifies that our optimized Martini force field is reliable.

The OPLS-AA force filed[36,37] consists of harmonic terms for bond stretching and angle bending, a Fourier series for each dihedral angle, and Coulombic and Lennard-Jones interactions between atoms separated by three or more bonds as shown in eq 1

$$
\begin{aligned}
E &= E_{\text{no−bond}} + E_{\text{bonds}} + E_{\text{angles}} + E_{\text{dihedral}} \\
&= \sum_i \sum_{j>i} \left[\frac{q_i q_j e^2}{r_{ij}} + 4\varepsilon_{ij} \left(\frac{\sigma_{ij}^{12}}{r_{ij}^{12}} - \frac{\sigma_{ij}^6}{r_{ij}^6} \right) \right] \\
&+ \sum_{\text{bonds}} K_r (r - r_{\text{eq}})^2 + \sum_{\text{angles}} K_\theta (\theta - \theta_{\text{eq}})^2 \\
&+ \sum_i \left\{ \frac{V_{1i}}{2} [1 + \cos(\varphi_i)] + \frac{V_{2i}}{2} [1 - \cos(2\varphi_i)] \right. \\
&\left. + \frac{V_{3i}}{2} [1 + \cos(3\varphi_i)] + \frac{V_{4i}}{2} [1 - \cos(4\varphi_i)] \right\}
\end{aligned}
\tag{1}
$$

The total energy E of the system is the sum of individual energies of Coulombic terms, Lennard-Jones terms, harmonic bond stretching terms, angle bending terms, and a Fourier series for torsional energetics. The partial atomic charge q is fixed on each atom's mass center, i and j represent all pairs of atoms ($i < j$), and r_{ij} is the distance between atoms i and j. ε_{ij} and σ_{ij} represent the Lennard-Jones radii and the potential well depth. K_r, K_θ, and V_{ni} ($n = 1, 2, 3, 4$) are the force constants and r_{eq}, θ_{eq}, and φ_i represent equilibrium values.

The Martini force filed[31,38] is given in eq 2. The angle bending terms and the Fourier series for torsional energetics is ignored. Therefore, the MD simulation based on the Martini force field is much faster than that based on the AA force field.

$$
\begin{aligned}
E &= E_{\text{non−bond}} + E_{\text{bonds}} \\
&= \sum_i \sum_{j>i} \left[\frac{q_i q_j e^2}{r_{ij}} + 4\varepsilon_{ij} \left(\frac{\sigma_{ij}^{12}}{r_{ij}^{12}} - \frac{\sigma_{ij}^6}{r_{ij}^6} \right) \right] \\
&+ \sum_{\text{bonds}} K_r (r - r_{\text{eq}})^2
\end{aligned}
\tag{2}
$$

In the coarse-grained molecular dynamics (CG MD) simulation, all of the beads have the same volume, radius, and mass. These bead parameters are obtained as follows. The size of a bead corresponds to four water molecules in the Martini force field,[31] where 4 to 1 is the law of coarse-grained mapping. The molar volume of water is 18 cm^3 mol^{-1}. Therefore, the volume of one water molecule is
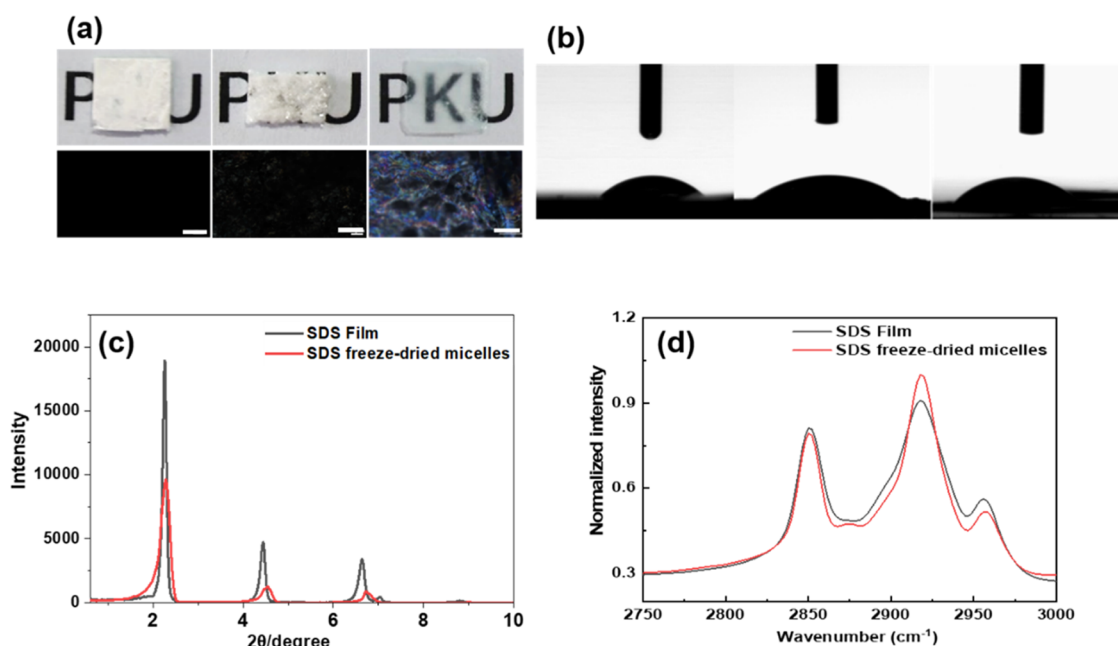
$$
v_{\text{water}} = \frac{18 \text{ cm}^3/\text{mol}}{6.02 \times 10^{23} \text{molecules}\cdot\text{mol}^{-1}} = 30 \text{ Å}^3
\tag{3}
$$

and the volume and mass of one water bead are

$$
v_{\text{b}} = 4v_{\text{water}} = 120 \text{ Å}^3
\tag{4}
$$

$$
m = 4m_{\text{water}}
\tag{5}
$$

where m is the mass of a bead and m_{water} is the mass of one water molecule (18 amu). Therefore, each bead has a mass of 72 amu. To define the diameter and radius of each bead, we use eqs 6 and 7[39]

Figure 1. Comparison of the experimental results of SDS film and other types of SDS solids. (a). Upper, from left to right: the photograph of pressed SDS commercial powders, SDS crystals, and SDS films. Lower: polarized optical microscopy (POM) of these samples. Bar represents 100 μm. (b) Contact angle of water on the samples in (a). (c) XRD results of SDS film and freeze-dried SDS micelles. (d) FT-IR results for SDS film and freeze-dried SDS micelles.

$$r_c^3 = \rho v_b \tag{6}$$

$$l_{box} = (\rho v_b)^{1/3} = 4.932\rho^{1/3} \text{ Å} \tag{7}$$

where l_{box} is the length of a cubic, v_b is the volume of one water bead defined by eq 4, and ρ is the number of beads in a cubic volume of length l_{box}. By choosing $\rho = 3$, a liquid with the compressibility of water is simulated.[39] According to eq 7, l_{box} = 7.11 Å, which corresponds to the diameter of each bead, and half of it is the radius of a bead, 3.56 Å. The volume of each bead is 120 Å³ (eq 4), and the mass of each bead is 72 amu (eq 5). In the simulations, the volume, size, and mass of the beads are maintained constant, which come from Martini 2.0.[38] All of the calculations are performed in a cubic simulation box with periodic boundary conditions applied in all directions. The enclosed system is composed of beads of water, dodecyl sulfate (SDS⁻), and hydrated sodium ions (Na⁺). The total number of beads in the system is given by

$$N_b = \frac{\rho V_{box}}{l_{box}^3} \tag{8}$$

where N_b is the total number of beads in the system, V_{box} is the total volume of the simulation box, and ρ is defined as the number of beads, or bead density, in a cubic volume of length l_{box} (see above), which is the diameter of a bead.

Several SDS concentrations have been calculated. To establish the number of SDS coarse-grained molecules required to ensure the desired concentration, we apply

$$C = \frac{N_S}{N_A V_{box}} \tag{9}$$

$$N_S = C N_A V_{box} \tag{10}$$

where C is the mole concentration (M, molar), N_S is the number of coarse-grained molecules of SDS, N_A is Avogadro's

number (6.02×10^{23} molecules mol⁻¹), and V_{box} is the volume of the box in liters.

The Martini CG potential is easier than an atomic potential such as OPLS[37] because of the simplification of the number of calculation units and various optimizations in the force field equation. Based on the comparison simulation time for atomic and coarse grain, it is found that the Martini computational efficiency is about 1000 times larger than the OPLS-AA simulation. All simulations are conducted using the open-source software package LAMMPS.[40] Structural figures and trajectory videos were prepared using VMD.[41] The initial configurations of the simulated systems are constructed to have a random distribution of water molecules while ensuring SDS molecules are distributed averagely in the entire volume.

3. RESULTS AND DISCUSSION

3.1. Experimental Results of SDS Self-Assembly in Solid Phase. Recently, Yan et al.[13] found that molecules in the precipitates formed with the aqueous mixture of ionic surfactant and oppositely charged polyelectrolyte may undergo self-assembly to form large-area self-supporting films under pressure in the presence of a tiny amount of water.[12−17] The driving forces for the multiscale self-assembly process are mainly the hydrophobic interaction between surfactant molecules. The electrostatic interaction between the polyelectrolyte chain and surfactant molecules is to endow the film with the self-supporting ability through the cross-linking of nanodomains formed by surfactants. Therefore, without polyelectrolyte, the nanodomains of surfactants are expected to still have the ability to undergo scale-span self-assembly in the solid phase but cannot form self-supporting films.

To test this hypothesis, three different SDS powders, namely, commercial SDS powders, SDS crystal powders obtained from the recrystallization of commercial SDS in an organic solvent, and the amorphous powder obtained from

Table 1. Simulation Details of SPMSA of the SDS–H$_2$O System in Martini CG Force Field[a]

mole ratio (H$_2$O/SDS)	N_s	N_w	d_{box} (Å)	C_{SDS} (M)
0	300	0	56.1	2.82
0.067	300	20	56.266	2.80
0.133	300	40	56.216	2.81
0.2	300	60	56.36	2.784
0.26	300	80	56.39	2.779
0.33	300	100	56.4	2.778
0.67	300	200	59	2.43
1	300	300	59.2	2.40
1.33	300	400	59.4	2.38
1.67	300	500	59.6	2.35
2	300	600	59.65	2.348
2.33	300	700	59.7	2.34
2.67	300	800	60	2.31
4	300	1200	60.8	2.22
8	300	2400	63.2	1.97
16	300	4800	68.5	1.55
32	300	9600	77.4	1.07
64	300	19,200	90.8	0.67
80	300	24,000	96.2	0.56
93	300	28,000	100.5	0.49

[a]N_s and N_w are the initial number of SDS and water molecules, respectively. d_{box} is the length along the $X/Y/Z$ direction of the simulated cubic box. C_{SDS} is the calculated concentration of SDS corresponding to each molar ratio between water and SDS.

freeze-dried aqueous SDS micellar solution, were employed as the model system for the study of the SPMSA. It can be seen from the photograph in Figure 1a that when the three SDS powders are compacted at a pressure of 8 MPa, only the powder of freeze-dried micelles is transformed into a transparent film upon dropping a small amount of water (Figure S4), while the other two solids remain as white cakes under the same condition. Control experiments revealed that all of the three powders have hydrophilic surfaces so that the contact angles of water on them are all less than 20° (Figure 1b). This means that the failed formation of film in the commercial powder and crystal SDS systems is not due to the difference in water diffusion from the surface to the internal. The XRD patterns for the films and the powder of freeze-dried micelles are similar, both giving typical diffractions for two-dimensional (2D) lamellar lattices (Figure 1c). However, the diffractions are strikingly intensified and sharpened after the freeze-dried SDS micelles are transformed into a film (Figure

1c), which indicates that the sizes of the SDS bilayers in the SDS film are much larger than that in the powder cake of the freeze-dried micelles.[13] Indeed, scanning electron microscopy (SEM) observation clearly shows the layered structures in the film (Figure S5). FT-IR results for the SDS film and freeze-dried SDS micelles reveal that the wavenumber of symmetric and asymmetric vibration of the hydrocarbon chains both occur at 2850 and 2918 cm^{-1} (Figure 1d), which is the feature of orderly packed SDS in bilayers. This means the formation of SDS films from freeze-dried micelles does not change the packing mode of SDS molecules. It is noticed that polarized optical microscopy (POM) images manifest strong birefringence only for the transparent SDS film (Figure 1a), indicating that neither the commercial SDS powder nor the crystallized SDS sample is able to form mesophases under conditions of SPMSA.

3.2. Simulation of SDS Self-Assembly in Solid Phase with Optimized Martini Force Field. Based on the above experimental results, and the qualified MD method using the optimized Martini CG force field in Section 2.2, we simulated and analyzed the molecular self-assembly process of SDS in the solid phase and systematically studied the effect of water, pressure, and the size of SDS aggregates in the sample formed by freeze-dried SDS micelles in this study.

3.2.1. Effect of the Molar Ratio of H$_2$O/SDS. To study the impact of water content on the SPMSA process, the molar ratio of H$_2$O/SDS is varied between 0:1 and 93:1. The initial states of these different systems are constructed to have a random distribution of water molecules but a uniform distribution of SDS molecules, as demonstrated by the moltemplate package[42] and PACKMOL package.[43] Simulation manifests that variation of initial water distribution has not much difference on the self-assembling behavior of SDS (Figure S6). The snapshots of the 1 ns NPT (a system with a fixed number N of molecules, 1 atm pressure P, and 300 K temperature T) simulation for systems with different water content (Table 1) are given in Figure 2.

The snapshots in Figure 2 reveal that in the H$_2$O/SDS molar ratio range of 0:1 to 0.26:1 with a small amount of water, the SDS domains cannot merge into lamellae, so the individual domain boundaries are clearly observed. This means if there is no sufficient water in the preassembled SDS powders, SPMSA cannot occur, which agrees well with our experimental results in Figure 1a. The calculation suggests that as the content of water is increased to reach the H$_2$O/SDS molar ratio of 0.33:1 to 1:1, the isolated SDS domains merge into continuous
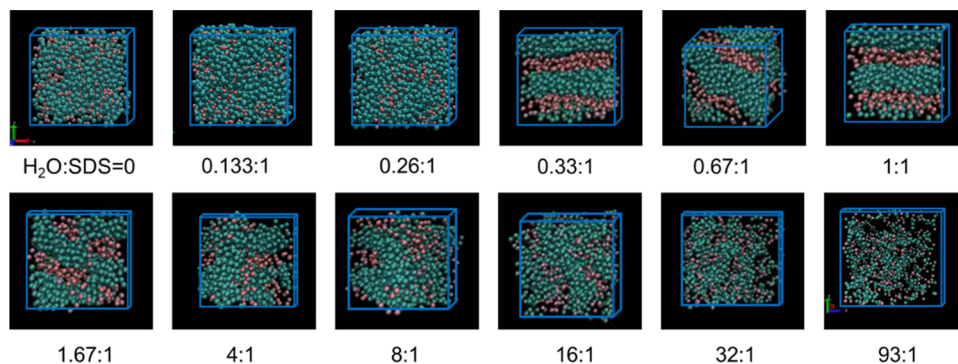
Figure 2. Snapshots of CG simulation at 1 ns for the SDS–H$_2$O systems (water is not shown) with varying water contents. The red bead is the SDS head group and the blue bead is the tail of SDS.
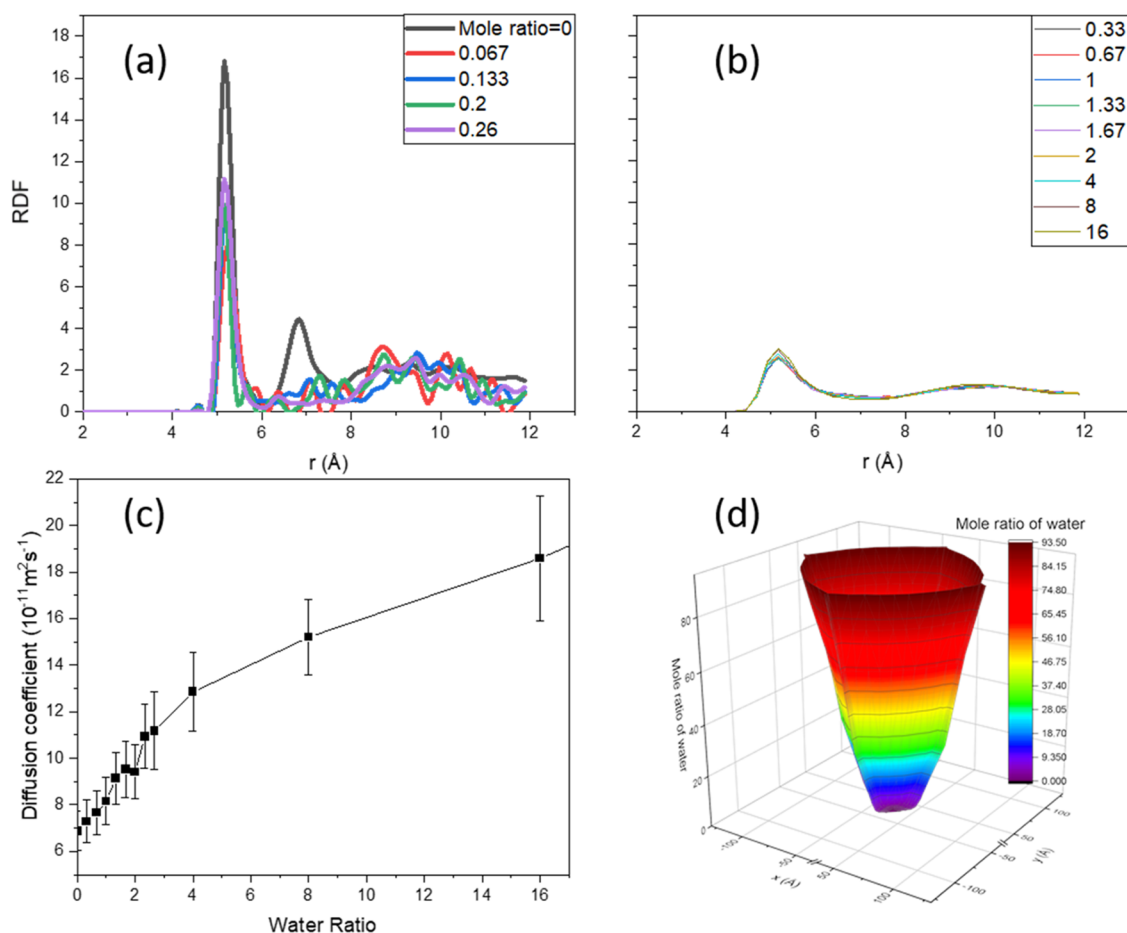
Figure 3. Quantitative analysis of CG simulation for SDS−H₂O systems at different water contents. (a) RDF at 4 ns in SPDMA (the range of 0:1 to 0.26). (b) RDF in the range of 1:0.33 to 1:16. (c) Diffusion coefficiency curve of SDS at different mole ratios of H₂O/SDS. (d) Diffusion range of SDS molecules in x- and y-directions at different mole ratios of H₂O/SDS.

**Table 2. Simulation Details of SPMSA of the SDS−H₂O System at Different Interparticle Distances[a]**

d (nm)	l_x (Å)	l_y (Å)	l_z (Å)	n	N_S	N_w
2	56.5	153	153	300	300	300
4	56.5	193	193	300	300	300
8	56.5	273	273	300	300	300
16	56.5	433	433	300	300	300
32	56.5	753	753	300	300	300

[a]d is the interparticle distance. l_x, l_y, and l_z are the box size in the xyz-directions, respectively. n, N_S, and N_w are the initial cluster size, the initial number of SDS, and the initial number of water molecules, respectively.

lamellae composed of SDS bilayers. Further increasing the content of water to the H₂O/SDS molar ratio range of 1.67:1 to 8:1, bicontinuous phases are formed. Both the lamellar phase and the bicontinuous phases are the result of SPMSA, indicating that this process may occur in the broad range of

H₂O/SDS molar ratio between 0.33:1 and 8:1. Indeed, experimental results reveal that the content of water may be about 12−16% (wt %) in some SPMSA systems.[17] It is noticed that the calculation results manifest that as the H₂O/SDS molar ratio exceeds 16:1, the system gives characteristic solution features, where the SDS molecules are dispersed in the whole system. In experiments, it is rational that the SDS finally forms a solution if enough water is added. These scenarios verify that the current MD simulations are reasonable in describing the SPMSA behavior of SDS.

To probe the molecular arrangement in the SDS systems with different water contents, the radial distribution function (RDF) between SDS molecules for the SDS−H₂O system was further analyzed. Figure 3a shows that as the mole ratio of H₂O/SDS is in the range of 0:1 to 0.26:1, multiple peaks occur and the peak position changes with the water content, indicating that the SDS molecules cannot form orderly arranged structures due to the lack of mobility. In contrast,
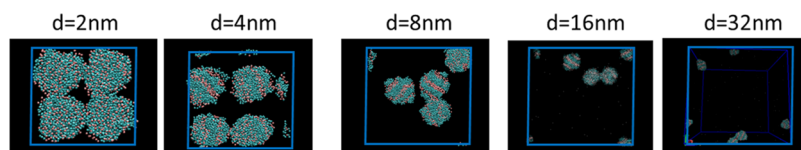
Figure 4. 3D snapshots of SPMSA at 4 ns at different cluster spacings.
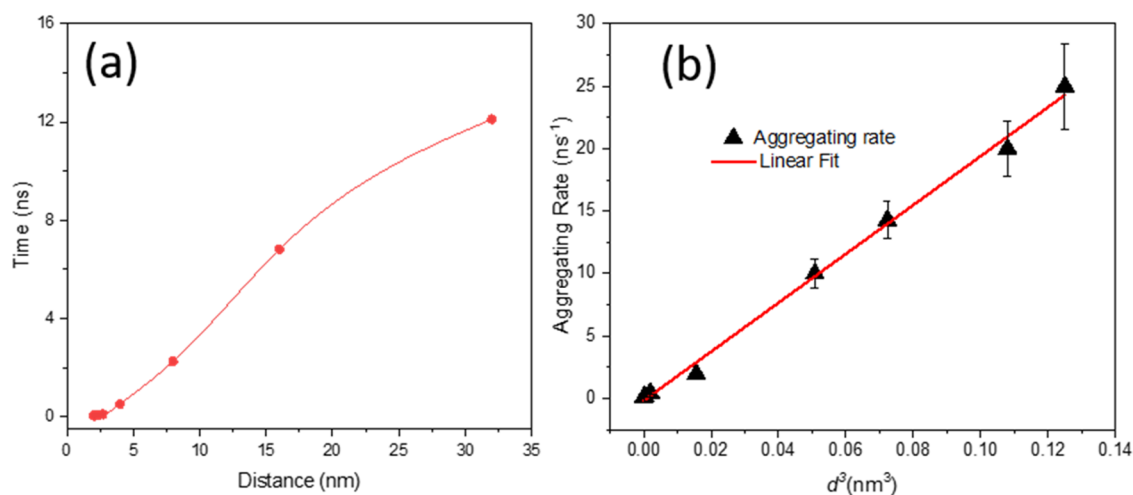
Figure 5. Relationship between the interparticle distance d of SDS domains and first collision time t in 4*(300SDS + 300H$_2$O) system. (a) Time vs distance. (b) R vs d^{-3} and the linear fit.

Table 3. Simulation Details of SPMSA of the SDS−H$_2$O System of Different Cluster Sizes[a]

n	d (nm)	N_S	N_w	l_x (Å)	l_y (Å)	l_z (Å)
150	8	150	150	56.5	240	240
300	8	300	300	56.5	273	273
1200	8	1200	1200	56.5	386	386
2400	8	2400	2400	56.5	480	480
4800	8	4800	4800	56.5	612	612
7500	8	7500	7500	56.5	725	725
150	16	150	150	56.5	400	400
300	16	300	300	56.5	433	433
1200	16	1200	1200	56.5	546	548
2400	16	2400	2400	56.5	640	640
4800	16	4800	4800	56.5	772	772
7500	16	7500	7500	56.5	845	845

[a]d is the interparticle distance. l_x, l_y, and l_z are the box size in the xyz-direction, respectively. n, N_S, and N_w are the initial cluster size, the initial number of SDS, and the initial number of water molecules, respectively.

as the H$_2$O/SDS molar ratio enters the region of 1:0.33 to 1:16 (Figure 3b), where the lamellae and bicontinuous phase are formed, double peaks can be obtained, indicating that the SDS molecules are self-assembled orderly into bilayer structures. Figure 3c shows the diffusion coefficients calculated from the MSD curves (Figure S7). It is clear that when the content of water is very low, the impact of water on the diffusion coefficient is much larger than that when the water content is high. This means that the presence of a small amount of water is very crucial for the SPMSA formation. As the content of

water is higher than a critical value, further increasing water would not produce a determinative impact on the SPMSA.

To better understand the microscopic picture of the diffusion ability of SDS, the diffusion range is calculated from the xy-coordinates at 4 ns using eq 11

$$\text{range} = \underset{i=1}{\overset{N}{\text{Max}}}\left(\sqrt{x_i^2 + y_i^2}\right) \tag{11}$$

where N is the bead number, i is the bead index, and x_i and y_i are the coordinates of the bead i. According to the diffusion range in x- and y-directions (Figure 3d), the formation of the SPMSA film only requires SDS molecules to move in a small amplitude of ± 50 Å at the bottom of the cuplike three-dimensional (3D) illustration of the diffusion range. Excess water is not required in the structure of the SPMSA film. However, in experiments, we have to drop much more excess water to facilitate sufficient SDS migration within a short time. The redundant water leaves the film via spontaneous evaporation. Of course, larger than this displacement of SDS facilitated by higher water content is also helpful for the SPMSA formation, but the excess water would be excluded from the system via evaporation to keep the system in the form of films.

3.2.2. Influence of Interparticle Distance on the SPMSA Behavior. In the experiment, pressure is required to achieve SPMSA. Since the pressure here is only of medium strength, we consider its role to compact the solids by shortening the interparticle distance. In the NVT MD simulation, the distance between the SDS domains is then studied to elucidate the role of pressure on SPMSA. The initial simulation details are given
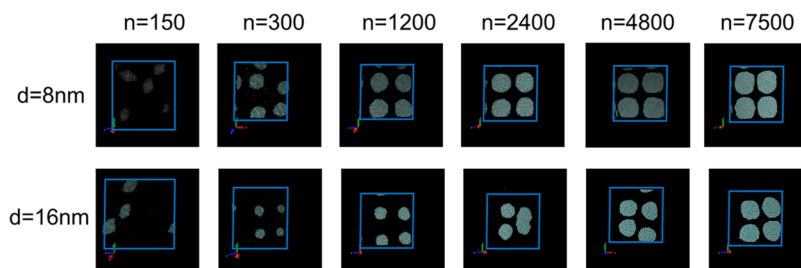
Figure 6. 3D snapshots at different cluster sizes in the SDS−H$_2$O SPMSA process when d = 8 and 16 nm are obtained at 4 ns.
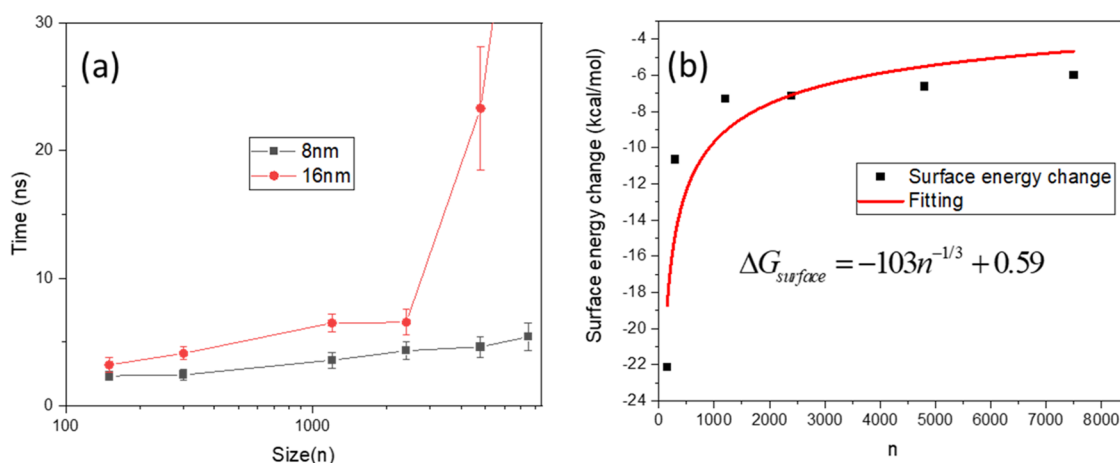
Figure 7. Analysis of CG simulation for the SDS−H$_2$O systems at different initial cluster sizes. (a) Relationship between starting collision time and unit size in the SDS−H$_2$O SPMSA system at two different interdomain distances. (b) Variation in surface energy change upon fusion of the SDS clusters with the individual cluster size of SDS calculated by simulation. The red line is the fitting curve based on the equation $y = An^{-1/3} + B$. The size n is expressed as the number of SDS molecules in each cluster.

in Table 2 and the 3D snapshots are shown in Figure 4. Each SDS domain is set to contain 300 SDS and 300 water. It is found that the first collision time t increases as the distance d becomes larger (Figure 5a). This agrees well with our experimental observations that increasing pressure enhances the ability of SPMSA formation.[13]

To quantitatively study the impact of the distances d between the clusters on the molecular self-assembly in the solid phase, we define the fusion rate R of the SDS domains as $R = 1/t$, where t is the minimum time required for the first collision of the two SDS domains. Figure 5b shows that the $R \sim d^{-3}$ plot gives a linear relationship, which can be described by the function of $R = 196d^{-3}$. Since d is the distance between two SDS domains, this function indicates that the fusion rate of the SDS domains can be drastically reduced by increasing the interdomain distance. This explains why experimentally external pressure is required for the self-assembly of SDS in solid states. It should be pointed out that the $R \sim d^{-3}$ relationship may be different for different systems in the SPMSA study.

3.2.3. Influence of Domain Size on the SPMSA Behavior. The experimental results in Figure 1 indicate that the size of the initial SDS domains in the solids is crucial for the occurrence of SPMSA. Then, the size of the SDS clusters varied by changing the number of SDS molecules in each SDS domain from 150 SDS + 150 H$_2$O to 7500 SDS + 7500 H$_2$O in CG MD simulation. The simulation details are given in Table 3, and the 3D snapshots at 4 ns in different cluster sizes are given in Figure 6.

The quantitative relationship between the fusion rate and domain size in Figure 7a shows that the distance between the domains has a great impact on the time required for the first collision. In the case of the interdomain distance being 8 nm, the collision time increases slowly with the increasing domain size. However, at the interdomain distance of 16 nm, the collision time increases sharply as the domain reaches a certain size. This means that fusion of the SDS domains does not occur anymore as the domain size exceeds a threshold.

The physical insight into the impact of SDS domain size on the SPMSA lies in the sharply reduced variation of Gibbs free energy (ΔG) with the increasing cluster size. Figure 7b shows the variation in Gibbs free energies accompanied by the cluster

fusion obtained from the simulation (Figure S8). The fix plumed command of LAMMPD package[44] was used to calculate the Gibbs free energies. It is clear that with the increasing cluster size, the fusion caused the reduction of Gibbs free energy reduces, making the fusion less energy favorable. Because the fusion of the SDS domains reduces the total surface area of the system, the surface Gibbs free energy of the system is decreased.

Theoretically, the total surface Gibbs free energy change[45] can be obtained from eq 12

$$\Delta G_{surface} = -\left(\frac{N_0}{n}\right)\left[4\pi\left(\frac{3v_0}{4\pi}\right)^{2/3}\right]\gamma n^{2/3}$$
$$= -4.84 N_0 \gamma v_0^{2/3} n^{-1/3} \qquad (12)$$

where N_0 is the total number of SDS molecules, n is the initial size of the cluster, and γ is the interfacial free energy per unit area. One first equates nv_0 to the volume of a cluster containing n SDS molecules and then uses this relation to factor $n^{2/3}$ to obtain the area of the SDS domain, presumably a sphere. Since N_0, γ, and v_0 are all constant in the SDS−H$_2$O system, the dimensionless surface Gibbs free energy change is proportional to $n^{-1/3}$. The red line in Figure 7b shows the fitting curve obtained on the basis of eq 12. It is clear that the simulation result (black squares) and the theoretical prediction (red line) agree very well with each other, and both show that the variation in the Gibbs free energy decreases drastically as the cluster size reaches a critical value of about 1000 SDS. This means that there is a critical cluster size (CCS) for the SPMSA. SPMSA occurs only when the domain size is smaller than this CCS. This explains the experimental observations that the SDS crystals and commercial powders do not undergo SPMSA under the same conditions as those for the freeze-dried SDS micelles. However, this CCS value should be different for different surfactant systems. For this reason, we do not look seriously at the absolute value for the thresh hold value of the domain size.

4. CONCLUSIONS

MD simulations based on the CG model for SPMSA of the SDS study confirm that water, pressure, size of the SDS

domains, and distance between the domains cooperatively facilitate the SPMSA. It reveals that the merging of the preassemblies occurs efficiently as the molar ratio of [SDS]/[H$_2$O] is in the range of 1:0.33 to 1:16, so a critical H$_2$O/SDS molar ratio of 1:0.33 is required for the occurrence of its SPMSA. Increasing the pressure could compact the amorphous solid of SDS; therefore, the drastically reduced interdomain distance would facilitate the SPMSA. The domain size of the surfactant is also very crucial for the SPMSA. The smaller the domain size, the faster the fusion of the domains. For large SDS domains with a large interdomain distance, failure of SPMSA is expected in the CG MD simulation. This MD study confirms our proposed picture for the experimentally observed SPMSA process, indicating that SPMSA is a thermodynamically favored process that would be generalized to a vast number of systems.

■ ASSOCIATED CONTENT

ⓢ Supporting Information

The Supporting Information is available free of charge at https://pubs.acs.org/doi/10.1021/acs.jpcb.2c04421.

> Comparison of the force field equation between OPLS and Martin, the OPLS-AA and Martini force field (Figures S1−S2, Tables S1−S3), the comparison of the diffusion coefficient of low-concentration SDS solutions with literature results (Figure S3), POM images for the film formation from the freeze-dried micelles (Figure S4), SEM image of the layered structures for the film (Figure S5), the impact of starting water distribution on the self-assembly of SDS (Figure S6), the MSD (mean square displacement) at different water ratios (Figure S7), and surface energy variation for a film contains clusters with different sizes (Figure S8) (PDF)

■ AUTHOR INFORMATION

Corresponding Authors

Bin Zhang − *College of Chemistry and Molecular Engineering, Peking University, Beijing 100871, China*; Email: binzhang@pku.edu.cn

Tao Chen − *College of Chemistry and Materials Science, Northwest University, Xian 710127, China*; ⓘ orcid.org/0000-0001-6686-1821; Email: tchen@nwu.edu.cn

Yun Yan − *College of Chemistry and Molecular Engineering, Peking University, Beijing 100871, China*; ⓘ orcid.org/0000-0001-8759-3918; Email: yunyan@pku.edu.cn

Authors

Xiangyu Dou − *College of Chemistry and Molecular Engineering, Peking University, Beijing 100871, China*; ⓘ orcid.org/0000-0003-4219-5777

Hongjun Jin − *College of Chemistry and Molecular Engineering, Peking University, Beijing 100871, China; Engineering Research Center of Polymer Green Recycling of Ministry of Education, College of Environmental Science and Engineering, Fujian Normal University, Fuzhou, Fujian 350007, China*

Tongyue Wu − *College of Chemistry and Molecular Engineering, Peking University, Beijing 100871, China*

Jianbin Huang − *College of Chemistry and Molecular Engineering, Peking University, Beijing 100871, China*

Zhirong Liu − *College of Chemistry and Molecular Engineering, Peking University, Beijing 100871, China*; ⓘ orcid.org/0000-0001-5070-8048

Complete contact information is available at:
https://pubs.acs.org/10.1021/acs.jpcb.2c04421

Author Contributions

∥Equal contributor.

Notes

The authors declare no competing financial interest.

■ ACKNOWLEDGMENTS

■ REFERENCES

(1) Gao, S. T.; Qi, J. W.; Jiang, S. S.; Wu, T. Y.; Wang, W. K.; Cai, Y. T.; Ma, C.; Zhang, B.; Huang, J. B.; Yan, Y. Green wood adhesives from one-pot coacervation of folic acid and branched poly(ethylene imine). *ACS Appl. Bio Mater.* **2021**, *4*, 7314−7321.

(2) Li, J. L.; Yuan, S.; Qin, J. S.; Pang, J. D.; Zhang, P.; Zhang, Y. M.; Huang, Y. Y.; Drake, H. F.; Liu, W. S. R.; Zhou, H. C. Stepwise assembly of turn-on fluorescence sensors in multicomponent metal-organic frameworks for in vitro cyanide detection. *Angew. Chem., Int. Ed.* **2020**, *59*, 9319−9323.

(3) Yamanoi, Y.; Nakae, T.; Nishihara, H. Bio-organic-inorganic hybrid soft materials: photoelectric conversion systems based on photosystem I and II with molecular wires. *Chem. Lett.* **2021**, *50*, 1263−1270.

(4) Chen, H. L.; Zhang, W. N.; Li, M. L.; He, G.; Guo, X. F. Interface engineering in organic field-effect transistors: principles, applications, and perspectives. *Chem. Rev.* **2020**, *120*, 2879−2949.

(5) Liao, P. L.; Huang, J. B.; Yan, Y.; Tang, B. Z. Clusterization-triggered emission (CTE): one for all, all for one. *Mater. Chem. Front.* **2021**, *5*, 6693−6717.

(6) Qi, W. L.; Wang, X. J.; Liu, Z. Y.; Liu, K. E. D.; Long, Y. F.; Zhi, W. W.; Ma, C.; Yan, Y.; Huang, J. B. Visual recognition of ortho-xylene based on its host-guest crystalline self-assembly with a-cyclodextrin. *J. Colloid Interface Sci.* **2021**, *597*, 325−333.

(7) Liu, T. B. Hydrophilic macroionic solutions: what happens when soluble ions reach the size of nanometer scale? *Langmuir* **2010**, *26*, 9202−9213.

(8) Escobar, L.; Ballester, P. Molecular recognition in water using macrocyclic synthetic receptors. *Chem. Rev.* **2021**, *121*, 2445−2514.

(9) Kumar, R.; Sharma, A.; Singh, H.; Suating, P.; Kim, H. S.; Sunwoo, K.; Shim, I.; Gibb, B. C.; Kim, J. S. Revisiting fluorescent calixarenes: from molecular sensors to smart materials. *Chem. Rev.* **2019**, *119*, 9657−9721.

(10) Liu, T. B.; Langston, M. L. K.; Li, D.; Pigga, J. M.; Pichon, C.; Todea, A. M.; Muller, A. Self-recognition among different polyprotic macroions during assembly processes in dilute solution. *Science* **2011**, *331*, 1590−1592.

(11) Niu, W. W.; Zhu, Y. L.; Wang, R.; Lu, Z. Y.; Liu, X. K.; Sun, J. Q. Remalleable, healable, and highly sustainable supramolecular polymeric materials combining superhigh strength and ultrahigh toughness. *ACS Appl. Mater. Interfaces* **2020**, *12*, 30805−30814.

(12) Wang, W. K.; Xie, M. Q.; Jin, H. J.; Zhi, W. W.; Liu, K.; Ma, C.; Liao, P. L.; Huang, J. B.; Yan, Y. The pressing-induced formation of a large-area supramolecular film for oil capture. *Mater. Chem. Front.* **2020**, *4*, 1530−1539.

(13) Jin, H. J.; Xie, M. Q.; Wang, W. K.; Jiang, L. X.; Chang, W. Y.; Sun, Y.; Xu, L. M.; Zang, S. H.; Huang, J. B.; Yan, Y.; Jiang, L. Pressing-induced caking: a general strategy to scale-span molecular self-assembly. *CCS Chem.* **2020**, *2*, 98−106.

(14) Liao, P. L.; Zang, S. H.; Wu, T. Y.; Jin, H. J.; Wang, W. K.; Huang, J. B.; Tang, B. Z.; Yan, Y. Generating circularly polarized luminescence from clusterization-triggered emission using solid phase molecular self-assembly. *Nat. Commun.* **2021**, *12*, No. 3020.

(15) Xie, M. Q.; Che, Y. X.; Liu, K.; Jiang, L. X.; Xu, L. M.; Xue, R. R.; Drechsler, M.; Huang, J. B.; Tang, B. Z.; Yan, Y. Caking-Inspired Cold Sintering of Plastic Supramolecular Films as Multifunctional Platforms. *Adv. Funct. Mater.* **2018**, *28*, No. 1803370.

(16) Wu, T. Y.; Gao, S. T.; Wang, W. K.; Huang, J. B.; Yan, Y. Wearable Sensors Based on Solid-Phase Molecular Self-Assembly: Moisture-Strain Dual Responsiveness Facilitated Extremely High and Damage-Resistant Sensitivity. *ACS Appl. Mater. Interfaces* **2021**, *13*, 41997−42004.

(17) Jin, H. J.; Ma, C.; Wang, W. K.; Cai, Y. T.; Qi, J. W.; Wu, T. Y.; Liao, P. L.; Li, H. P.; Zeng, Q.; Xie, M. Q.; et al. Using molecules with superior water-plasticity to build solid-phase molecular self-assembly: room-temperature engineering mendable and recyclable functional supramolecular plastics. *ACS Mater. Lett.* **2022**, *4*, 145−152.

(18) Sosso, G. C.; Chen, J.; Cox, S. J.; Fitzner, M.; Pedevilla, P.; Zen, A.; Michaelides, A. Crystal nucleation in liquids: open questions and future challenges in molecular dynamics simulations. *Chem. Rev.* **2016**, *116*, 7078−7116.

(19) Pavošević, F.; Culpitt, T.; Hammes-Schiffer, S. Multi-component quantum chemistry: integrating electronic and nuclear quantum effects via the nuclear-electronic orbital method. *Chem. Rev.* **2020**, *120*, 4222−4253.

(20) Martin, M. G. Comparison of the AMBER, CHARMM, COMPASS, GROMOS, OPLS, TraPPE and UFF force fields for prediction of vapor-liquid coexistence curves and liquid densities. *Fluid Phase Equilib.* **2006**, *248*, 50−55.

(21) Nahar, A.; Baker, A. L.; Nichols, D. S.; Bowman, J. P.; Britz, M. L. Benchmarking DNA extraction methods for phylogenomic analysis of sub-antarctic rhodococcus and williamsia species. *Microorganisms* **2021**, *9*, No. 19.

(22) Berr, S. S.; Jones, R. R. M. Effect of added sodium and lithium chlorides on intermicellar interactions and micellar size of aqueous dodecyl-sulfate aggregates as determined by small-angle neutron-scattering. *Langmuir* **1988**, *4*, 1247−1251.

(23) Bezzobotnov, V. Y.; Borbely, S.; Cser, L.; Farago, B.; Gladkih, I. A.; Ostanevich, Y. M.; Vass, S. Temperature and concentration-dependence of properties of sodium dodecyl-sulfate micelles determined from small-angle neutron-scattering experiments. *J. Phys. Chem. A* **1988**, *92*, 5738−5743.

(24) López, C. A.; Rzepiela, A. J.; de Vries, A. H.; Dijkhuizen, L.; Hünenberger, P. H.; Marrink, S. J. Martini coarse-grained force field: extension to carbohydrates. *J. Chem. Theory Comput.* **2009**, *5*, 3195−3210.

(25) Lin, H.; Truhlar, D. G. QM/MM: what have we learned, where are we, and where do we go from here? *Theor. Chem. Acc.* **2007**, *117*, 185−199.

(26) Kaminski, G. A.; Friesner, R. A.; Tirado-Rives, J.; Jorgensen, W. L. Evaluation and reparametrization of the OPLS-AA force field for proteins via comparison with accurate quantum chemical calculations on peptides. *J. Phys. Chem. B* **2001**, *105*, 6474−6487.

(27) Dodda, L. S.; Vilseck, J. Z.; Tirado-Rives, J.; Jorgensen, W. L. 1.14*CM1A-LBCC: localized bond-charge corrected CM1A charges for condensed-phase simulations. *J. Phys. Chem. B* **2017**, *121*, 3864−3870.

(28) Dodda, L. S.; Cabeza de Vaca, I.; Tirado-Rives, J.; Jorgensen, W. L. LigParGen web server: an automatic OPLS-AA parameter generator for organic ligands. *Nucleic Acids Res.* **2017**, *45*, W331−W336.

(29) Harder, E.; Damm, W.; Maple, J.; Wu, C.; Reboul, M.; Xiang, J. Y.; Wang, L.; Lupyan, D.; Dahlgren, M. K.; Knight, J. L.; et al. OPLS3: a force field providing broad coverage of drug-like small molecules and proteins. *J. Chem. Theory Comput.* **2016**, *12*, 281−296.

(30) Kahn, K.; Bruice, T. C. Parameterization of OPLS-AA force field for the conformational analysis of macrocyclic polyketides. *J. Comput. Chem.* **2002**, *23*, 977−996.

(31) Souza, P. C. T.; Alessandri, R.; Barnoud, J.; Thallmair, S.; Faustino, I.; Grünewald, F.; Patmanidis, I.; Abdizadeh, H.; Bruininks, B. M. H.; Wassenaar, T. A.; et al. Martini 3: a general purpose force field for coarse-grained molecular dynamics. *Nat. Methods* **2021**, *18*, 382−388.

(32) Hussain, A. I.; Nasr, H. E.; El-Saadany, S. S.; El-Hamouly, S. H. Evaluation of the stability of emulsified ethylene-propylene-diene-monomer using novel technique. *J. Dispersion Sci. Technol.* **2010**, *31*, 1278−1284.

(33) Pitois, O.; Fritz, C.; Vignes-Adler, M. Liquid drainage through aqueous foam: study of the flow on the bubble scale. *J. Colloid Interface Sci.* **2005**, *282*, 458−465.

(34) Deng, Z.; Lü, H.; Leaist, D. G. Mutual diffusion coefficients and resistance coefficients for aqueous solutions of sodium alkanoate surfactants. *J. Chem. Eng. Data* **1996**, *41*, 214−217.

(35) Ribeiro, A. C. F.; Lobo, V. M. M.; Azevedo, E. F. G.; da G Miguel, M.; Burrows, H. D. Diffusion coefficients of sodium dodecylsulfate in aqueous solutions of sucrose and in aqueous solutions. *J. Mol. Liq.* **2001**, *94*, 193−201.

(36) Damm, W.; Frontera, A.; TiradoRives, J.; Jorgensen, W. L. OPLS all-atom force field for carbohydrates. *J. Comput. Chem.* **1997**, *18*, 1955−1970.

(37) Jorgensen, W. L.; Maxwell, D. S.; TiradoRives, J. Development and testing of the OPLS all-atom force field on conformational energetics and properties of organic liquids. *J. Am. Chem. Soc.* **1996**, *118*, 11225−11236.

(38) Marrink, S. J.; Risselada, H. J.; Yefimov, S.; Tieleman, D. P.; de Vries, A. H. The MARTINI force field: coarse grained model for biomolecular simulations. *J. Phys. Chem. B* **2007**, *111*, 7812−7824.

(39) Groot, R. D.; Warren, P. B. Dissipative particle dynamics: bridging the gap between atomistic and mesoscopic simulation. *J. Chem. Phys.* **1997**, *107*, 4423−4435.

(40) Plimpton, S. Fast parallel algorithms for short-range molecular dynamics. *J. Comput. Phys.* **1995**, *117*, 1−19.

(41) Humphrey, W.; Dalke, A.; Schulten, K. VMD: Visual molecular dynamics. *J. Mol. Graphics Modell.* **1996**, *14*, 33−38.

(42) Jewett, A. I.; Stelter, D.; Lambert, J.; Saladi, S. M.; Roscioni, O. M.; Ricci, M.; Autin, L.; Maritan, M.; Bashusqeh, S. M.; Keyes, T.; et al. Moltemplate: a tool for coarse-grained modeling of complex biological matter and soft condensed matter physics. *J. Mol. Biol.* **2021**, *433*, No. 166841.

(43) Martínez, L.; Andrade, R.; Birgin, E. G.; Martinez, J. M. PACKMOL: a package for building initial configurations for molecular dynamics simulations. *J. Comput. Chem.* **2009**, *30*, 2157−2164.

(44) Thompson, A. P.; Aktulga, H. M.; Berger, R.; Bolintineanu, D. S.; Brown, W. M.; Crozier, P. S.; in't Veld, P. J.; Kohlmeyer, A.; Moore, S. G.; Nguyen, T. D.; et al. LAMMPS—a flexible simulation tool for particle-based materials modeling at the atomic, meso, and continuum scales. *Comput. Phys. Commun.* **2022**, *271*, No. 108171.

(45) Agarwal, V.; Peters, B. Solute precipitate nucleation: a review of theory and simulation advances. *Adv. Chem. Phys.* **2014**, *155*, 97−159.